PAPER • **OPEN ACCESS**

Carrier transport and electronic defects in gallium oxide studied by photoconductivity techniques

To cite this article: Steve Reynolds *et al* 2025 *J. Phys.: Conf. Ser.* **2952** 012001

Journal of Physics: Conference Series **2952** (2025) 012001 doi:10.1088/1742-6596/2952/1/012001

Carrier transport and electronic defects in gallium oxide studied by photoconductivity techniques

Steve Reynolds[1*], David Nicol[2], Matthew Smith[3], Arpit Nandi[3], Sai Charan Vanjali[3], Martin Kuball[3] and Fabien Massabuau[2]

[1] School of Science and Engineering, University of Dundee, Dundee DD1 4HN, UK
[2] Department of Physics, SUPA, University of Strathclyde, Glasgow G4 0NG, UK
[3] Centre for Device Thermography and Reliability, H. H. Wills Physics Laboratory, University of Bristol, Bristol BS8 1TL, UK

[*]E-mail: s.z.reynolds@dundee.ac.uk

Abstract. Two complementary localised density of states spectroscopies, Modulated Photo-Conductivity (MPC) and the Constant Photocurrent Method (CPM) are applied to Ga_2O_3 thin films and are shown to be sensitive to carrier traps above and below the Fermi level, respectively. These techniques measure the film directly, without requiring a Schottky or p-n junction, which may offer advantages over conventional techniques in the study of high-resistivity or semi-insulating materials. The benefits of a higher-resolution MPC analysis are demonstrated.

1. Introduction

1.1 Applications summary

Interest in gallium oxide (Ga_2O_3), a wide-bandgap semiconductor ($E_G \sim 5$ eV), has gathered pace over recent years, stimulated by the prospect of applications in the energy and environmental sectors, as illustrated in Figure 1. These include: Power [1, 2] and RF [3] electronics; Solar-blind photodetectors [4, 5]; Photocatalysis [6]; Gas sensing [7].

Applications of gallium oxide in electronics and sensing are supported by the following merits:

- High breakdown field (*ca.* 8-10 MV/cm), due to strong Ga-O chemical bonds;
- High operating temperatures possible, due to low intrinsic carrier density;
- Peak optical sensitivity in the UVC spectral range (250 nm) – as minimal solar radiation below 250 nm reaches Earth's surface, the environment appears dark.
- Efficient, controllable n-type doping to $>10^{20}$ cm^{-3} (Si, Sn, Ge are shallow donors);
- Wide range of thin-film deposition techniques available;
- Single-crystal wafers (~2 inch diameter) of good electronic quality can be manufactured;
- Acceptable electron mobility (>100 cm^2/Vs) and high saturation velocity (2×10^7 cm/s);
- Heterojunctions permit design of high-mobility 2D electron gas devices;

Set against these are a number of challenges:

- Poor thermal conductivity impacts design of (particularly integrated) power devices;
- Low hole mobility and hole self-trapping, particularly at lower temperatures;
- p-type doping of Ga_2O_3 is proving difficult to achieve.

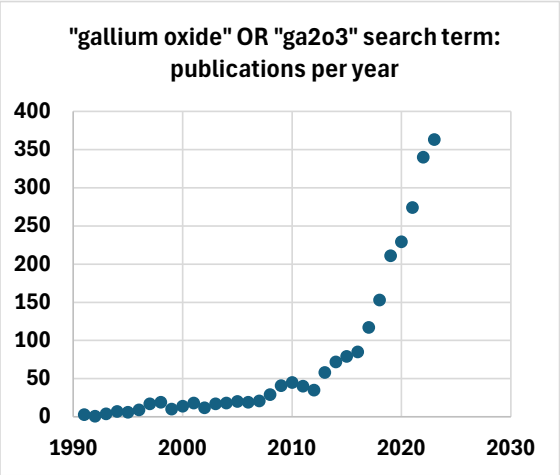

AND <phrase>	# pubs	%
transistor	964	36
"solar blind"	660	25
photocataly*	356	13
"gas sens*"	244	9
"transparent conduct*"	230	9
"solar cell*" OR PV	165	6
scintillat*	59	2
Total:	**2678**	**100**

Figure 1. Growth of research publications in the field of gallium oxide over the past 30 years. The table identifies major sub-topics featuring within the survey period (Scopus).

Although gallium oxide exists as several polytypes, most studies have focused on the monoclinic β-phase, which has an energy bandgap of 4.8 eV, remains stable up to high temperatures and single-crystals may be grown from the melt. The rhombohedral α-phase forms stable films at moderate temperatures when grown heteroepitaxially on a sapphire substrate, and has the highest bandgap of 5.3 eV. Further information and current research directions may be found in the literature cited above, and from additional reviews [8, 9].

1.2 Electronic defects

Localised electronic states (often referred to as traps) are present in all semiconductors to a greater or lesser extent [10]. As their name suggests, traps capture carriers, normally from the conduction band CB (electrons) or valence band VB (holes), where they remain until they are thermally emitted back to the band. Although trapped carriers are immobilised, they still contribute to space charge. Traps may be attributed to imperfections in crystal structure such as vacancies and interstitial atoms, dangling (unsatisfied) bonds, distorted bond lengths and angles in disordered materials, and impurity atoms. Differing local atomic environments arising due to a degree of disorder will tend to broaden the energy range over which a given species of localised state may extend. Distortion of 'strong' bonds leads to band tails, a set of shallow traps exponentially distributed with energy, extending into the band gap at the CB and VB edges.

Traps deep in the semiconductor bandgap are mostly undesirable. They may act as efficient recombination (Shockley-Read-Hall or SRH) centres, and increased recombination of excess carriers via this pathway may reduce the gain of amplifying devices and photoconductive sensors [11]. Emission from traps in the depletion layers of Ga_2O_3 Schottky power diode rectifiers increases leakage current, and the presence of traps is known to be a locus for instability and damage in Schottky diodes, transistors and UV LEDs [12, 13]. Carriers trapped in states other than recombination centres may be restricted from recombining, which may greatly extend the response time of photo-conductive detectors to light pulses [14].

To improve semiconductor quality on a systematic basis, it is useful to map the presence of localised states, in terms of their energy depth, capture properties and density (number per unit volume), and to seek to associate given species of trap with specific structural imperfections.

These might then be reduced by modifying materials preparation and device processing. In the case of gallium oxide, the two most common techniques for localised state characterisation are Deep Level Transient Spectroscopy (DLTS) and Deep Level Optical Spectroscopy (DLOS) [15, 16]. Both techniques detect charge emitted from traps within the depletion layer of (in the case of Ga_2O_3) a Schottky junction formed by a metal to n-type Ga_2O_3 contact, as an (often very small) change in junction capacitance or reverse current. In DLTS, traps in the depletion layer are firstly filled, normally by a forward bias pulse. In DLOS, the trap occupancy is controlled by a monochromatic light source, tuned to select either trap emptying (electrons from filled (acceptor-like) traps promoted into the CB) or trap filling (electrons from filled states in the VB transferred to an empty trap). Both transitions change the space charge density within the depletion layer, and hence may be detected similarly as for DLTS. However, to establish a Schottky barrier depletion layer within a given sample thickness a minimum space-charge width, and hence dopant concentration, is necessary. This may compromise the study of traps in high-resistivity thin films using DLTS.

DLTS has been developed to enable traps between 0.1 and 1.3 eV of the conduction band (CB) edge E_C in wide-bandgap materials such as n-type Ga_2O_3 to be studied but it is unsuitable for probing acceptor states in this material due to low hole mobility and a tendency for holes to remain self-trapped. Provided setup and detection parameters are chosen suitably, DLOS can detect both donor- and acceptor-like defects, thereby covering most of the bandgap. Other somewhat related techniques [14] include Thermally Stimulated Currents (TSC) and Photo-Induced Current Transient Spectroscopy (PICTS).

In the remainder of this paper, we introduce and demonstrate the effectiveness of two long-established but largely neglected defect spectroscopies [17], termed Modulated Photocurrent Spectroscopy (MPC) and Constant Photocurrent Method (CPM). Both techniques were developed in the study of defects in thin-film semiconductors such as thin-film silicon, CdS, CdSe, CdTe and CIGS, but more recently have found use in a wider range of materials including perovskites, organic semiconductors and some oxide semiconductors [18, 19].

1.3 Modulated Photo-Current Spectroscopy (MPC)

MPC is a defect spectroscopy technique utilising the amplitude and phase of the ac photocurrent when a semiconductor sample is illuminated by an amplitude-modulated normally above-gap light source. The sample has ohmic contacts, and is placed under an external voltage bias. In our laboratory, measurements may be taken typically between 0.1 Hz and 10 kHz, with the sample located in a cryostat to enable the temperature to be varied between 100 K and 450 K [17].

Carrier trapping and emission rates are related to trap density and energy depth, respectively. Imagine there is one species of electron trap, at an energy E_T below E_C. At sufficiently low modulation frequency f the emission time τ_e from this trap is much shorter than the period of the modulation, and electrons are thermally emitted to the CB shortly after being trapped. The ac photocurrent amplitude I_{ac} will therefore be maximal, and almost in phase with the modulation. As f is increased, emission is subject to significant delay, I_{ac} falls and a phase lag ϕ is visible. Continued increase in f leads to further reduction in I_{ac}, and ϕ approaches 90 degrees. A function $\sin(\phi)$ / I_{ac}, where $\phi = \tan^{-1}(2\pi f\tau_e)$, will therefore peak when the phase lag is 45 degrees, and approach zero at low and at high frequency. At $\omega_T = 2\pi/\tau_e$ the modulation is 'tuned' to the trap at energy depth $E_T = kT \ln(\nu/\omega_T)$, where ν is the attempt-to-escape frequency. The area under the peak is related to the number of traps at this energy per unit volume, or trap density N_T. Repeating the experiment at different temperatures will vary τ_e, allowing E_T and ν to be deduced from the

slope and intercept of an Arrhenius plot of ln(ω_T) vs. 1/T. More generally, by solving the ac rate equations, methods of resolving electron trap species distributed in energy above the Fermi level have been developed.

1.4 Constant Photo-Current Method (CPM)

CPM [17, 20] is both a defect spectroscopy and a highly-sensitive means of measuring the optical absorption coefficient α of a semiconductor thin film. It is often difficult to measure α for a thin film by subtractive optical means, especially at longer wavelengths, as the absorbed component may be much smaller than the measurement uncertainty in the reflected and transmitted components. CPM is based directly upon measurement of the photocurrent generated solely by the absorbed component, and so does not suffer from this limitation.

In the CPM experiment, a monochromatic, tuneable source of light is incident on the semiconductor sample, with ohmic contacts held at a constant potential difference. The photon energy E_P is gradually increased, but a photocurrent I_P will only flow if electrons can be promoted from the valence band, or from filled localised states in the band gap, to transport states in the CB beyond the band edge E_C. The mid-gap DOS in most semiconductors is small and at low E_P few photogenerated electrons are promoted into the CB. If the photon energy is increased and a set of traps is present at $E_T = E_C - E_P$, it may be detected by an increase in I_P. This component of photocurrent persists as E_P is further increased, even if the DOS subsequently drops to zero, provided $E_P > (E_C - E_T)$. Thus a series of discrete trap species, arranged in ascending energy intervals in the bandgap, should manifest as a 'staircase' rise in I_P as E_P is increased.

The CB edge is a fairly sharp energy probe, and as a first attempt, the trap DOS profile between the valence band edge E_V and the Fermi-level may be resolved by differentiating I_P vs. E_P (or more correctly, from $\mathrm{d}\alpha/\mathrm{d}E_P$). These filled states are inaccessible to MPC, and vice-versa. It follows that I_P reflects a convolution of the DOS subject to occupancy and energy conservation.

The eponymous 'constant photocurrent' in the abbreviation CPM concerns the experimental refinement [20] essential for accurate measurement of α, described more fully in section 2.2.

2. Experimental

2.1 MPC set-up, sample preparation and data processing

The sample studied was an unintentionally doped (UID) β-Ga_2O_3 film of thickness 350 nm deposited onto a *c*-plane sapphire substrate using an Agnitron Agilis 100 MOCVD tool [21]. Contacts were made using 2 mm × 1.5 mm Indium pads, with a nominal inter-electrode gap of 1 mm. Both dark and illuminated I-V characteristics over the range ±210 V were measured and found to be linear. From measurements taken at 10K intervals between 340K and 410K, the dark current activation energy was determined from Arrhenius plots to be 1.01 ± 0.03 eV. This implies that the equilibrium Fermi level of our sample was positioned a similar energy below E_C.

The MPC spectrometer set-up [22] is shown in Figure 2. The sample was mounted in a shop-made cryostat and illuminated through a quartz window by a 285 nm LED (Thorlabs LED285J). The dc optical intensity at the sample was approximately 0.5 mW cm^{-2}, with an ac (modulation) component of 0.035 mW cm^{-2}. The film absorption coefficient at 285 nm was 500 cm^{-1}, giving a rms ac carrier generation rate of 2.5×10^{16} cm^{-3} s^{-1}. In calculating the DOS according to equations (1) and (2) values of μ_e = 100 cm^2/Vs and $N_C = 3\times10^{18}$ cm^{-3} were adopted [8].

The key experimental data recorded in the MPC experiment are: (i) $I(\omega)$, the rms photocurrent amplitude, and (ii) $\phi(\omega)$, the phase lag between the photocurrent and the

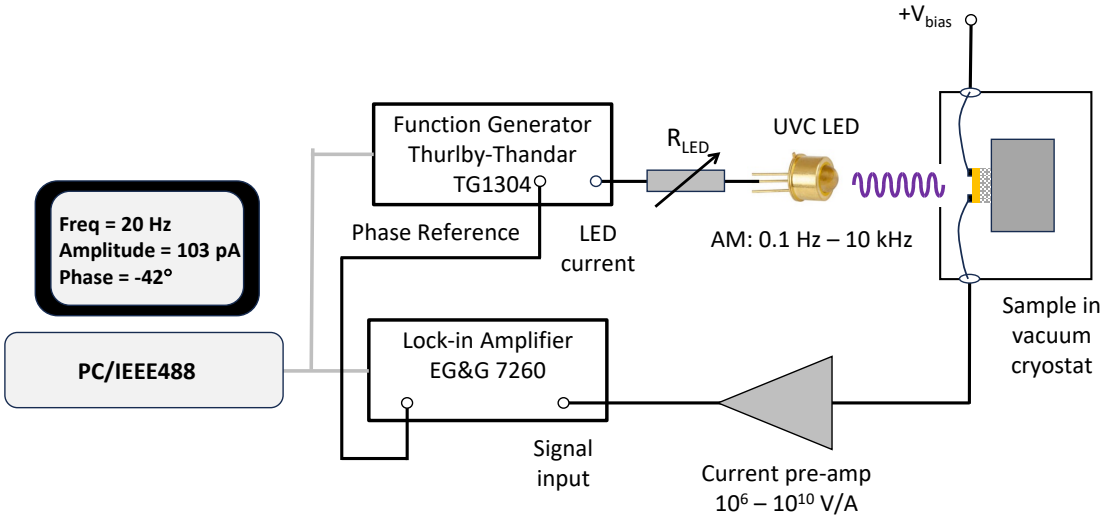

Figure 2. MPC set-up. The cryostat is shop-made and covers 100-420 K. The LED is available from Thorlabs (part number LED285J). The preamp is built around a Burr-Brown OPA637 IC.

modulation. Equations (1) and (2), developed by Brüggemann *et al* [23] and Hattori *et al* [24] respectively, connect these data to the localised DOS at an energy E_ω defined by equation (3):

$$N_{tB}(E_\omega) = \frac{2q\mu\varepsilon A_c G_\omega}{C_n \pi kT}\left[\frac{\sin(\phi(\omega))}{I(\omega)}\right] \text{ cm}^{-3}\text{eV}^{-1} \quad (1)$$

$$N_{tH}(E_\omega) = \frac{q\mu_e \varepsilon A_c G_\omega}{C_n kT}\left\{\omega \frac{d}{d\omega}\left[\frac{\cos(\phi(\omega))}{I(\omega)}\right]\right\} \text{ cm}^{-3}\text{eV}^{-1} \quad (2)$$

$$E_\omega = kT \ln(\nu/\omega) \quad (3)$$

Here q is the charge on the electron, k Boltzmann's constant, ω the modulation angular frequency, μ_e the band mobility, ε the electric field strength, A_c the conduction cross-sectional area, C_n the capture coefficient of the trap state and ν the attempt to escape frequency. E_ω is the energy of a trap species relative to the band edge. C_n and ν are connected by detailed balance considerations to N_C, the effective density of states in the CB, by:

$$C_n = \nu/N_C \quad (4a)$$

The capture cross-section of the trap is:

$$\sigma_n = C_n/\upsilon_{th} \quad (4b)$$

where υ_{th} is the electron thermal velocity.

2.2 CPM set-up, sample preparation and data processing

The sample comprised a film of UID α-Ga_2O_3 of thickness 250 nm deposited on *c*-plane sapphire substrates at a temperature of 250 °C by plasma-enhanced atomic layer deposition (PEALD) using

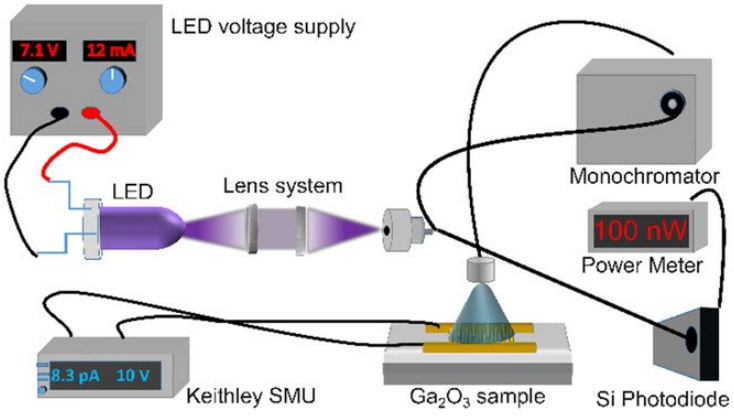

Figure 3. CPM set-up. LEDs from 465 nm to 250 nm are used as optical sources. The LED power supply plus neutral density filters are used to control intensity. Light is transmitted via optical fibres. The photocurrent is monitored using the Keithley SMU and is reset to the chosen constant value following each wavelength step. Reprinted with permission from [27].

an Oxford Instruments OpAL PEALD reactor [25]. Films were processed into photodetector structures by depositing interdigitated Ti (20 nm)/Au (80 nm) ohmic contacts [26].

The CPM spectrometer set-up is shown in Figure 3. The operating procedure is described in detail elsewhere [27], and the basic approach is as follows: The monochromator is set at the initial wavelength (typically 465 nm) and an appropriate LED selected. By adjusting the LED current and neutral density filters the sample photocurrent is set at the chosen constant value and the flux required is recorded. The monochromator is then decremented, typically by 3 nm, and the process continued, maintaining a constant photocurrent with the above adjustments and changing the LED when necessary until the full bandgap range is covered (typically to 250 nm).

Equation (5) relates the average photoconductivity $\Delta\sigma$ to the film optoelectronic parameters:

$$\Delta\sigma = \eta\Phi(1-R)\frac{(1-\exp(-\alpha d))}{d}q\tau_n\mu_n \approx \eta\Phi(1-R)\alpha q\tau_n\mu_n \quad (\text{for } \alpha d < 1) \tag{5}$$

Here η is the quantum efficiency, Φ the photon flux per unit area incident on the sample, R the reflection coefficient, α the optical absorption coefficient, d the film thickness, q the charge on the electron, τ_n the free electron lifetime and μ_n the electron mobility. For sub-bandgap excitation, ($\alpha d < 1$), η, μ_n and R do not vary significantly with photon energy. If a constant photocurrent (or photoconductivity) is actively maintained by adjusting Φ at each photon energy, the semiconductor quasi-Fermi levels remain fixed, which ensures a constant τ_n at each measurement step. Equation (6) may then be written:

$$\alpha(E_P) = \frac{Constant}{\Phi(E_P)} \tag{6}$$

where E_P is the photon energy. Equation (6) is calibrated by matching the α vs. E_P curve to that obtained using a proprietary optical spectrophotometer, in the spectral region where both methods are valid ($\alpha d \sim 1$).

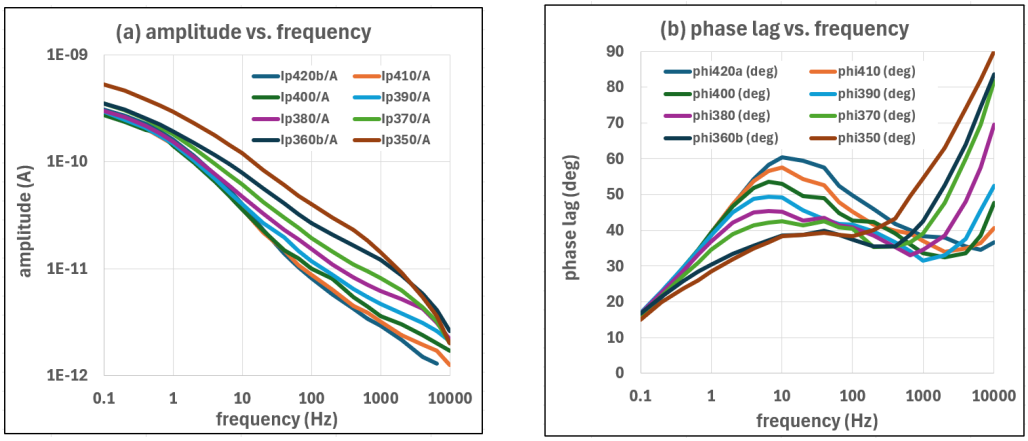

Figure 4. (a) Amplitude and (b) phase lag of photocurrent vs. frequency, between 350 K and 420 K.

3. Results and Discussion

3.1 MPC spectroscopy on β-Ga_2O_3

Figure 4 shows the ac signal amplitude (a) and the phase lag (b) vs. log frequency, parametric in temperature between 350 K and 420 K. The ac amplitude decreases monotonically with increasing frequency at a given temperature. This is expected, since as the frequency is increased a smaller proportion of the current of trapped electrons generated by the ac modulation will retain phase coherence when emitted. The phase lag plots reveal two distinct features; a broad peak between 1 and 100 Hz followed by a rapid rise towards 90° between 100 Hz and 10 kHz.

The DOS vs. energy relationships computed using equations (1-3) are shown in figures 5(a) and 5(b) respectively. An attempt to escape frequency ν of 9×10^{11} s^{-1} and energy corresponding to the prominent peak in Figure 5(b) (0.65 eV) were determined by selecting the value of ν giving the best agreement in peak position across the temperature range, in accordance with equation

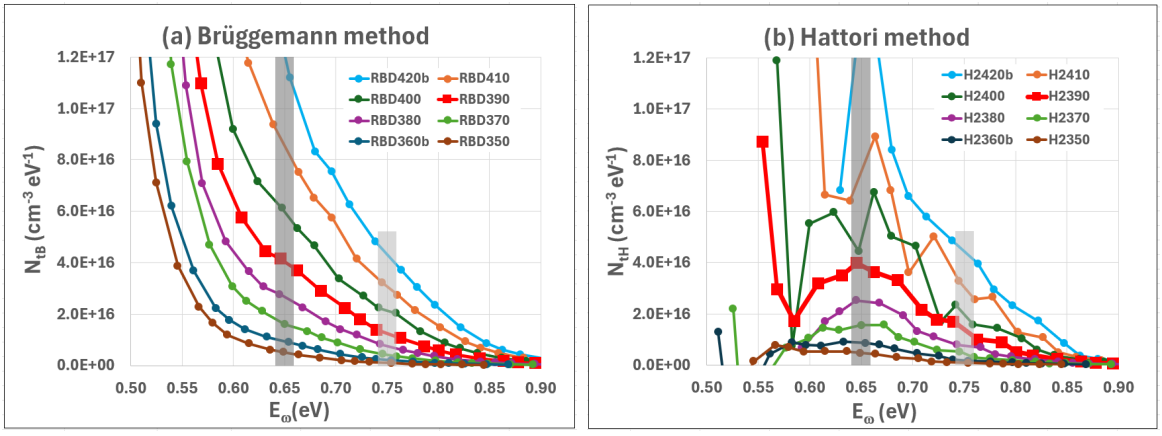

Figure 5. MPC DOS vs. energy using (a) Brüggemann and (b) Hattori (derivative) analysis methods. Higher resolution offered by Hattori method reveals peak (0.65 eV) and shoulder (0.75 eV) marked by thick grey lines, which are barely visible using Brüggemann method.

(3). A capture coefficient C_n = 2.3×10^{-7} cm^3 s^{-1} and cross-section σ_n = 2.3×10^{-15} cm^2 were then calculated from equations (4a) and (4b).

Although figures 5(a) and 5(b) utilise the same data set, they clearly differ very significantly. A peak feature is evident in figure 5(b), obtained using the higher-resolution Hattori analysis. Examining figure 5(a) closely, an inflection at 0.65 eV is visible in some of the curves. It therefore appears that the higher resolution of the Hattori method is essential to enable the peak to be distinguished from adjacent background features, which has not been reported previously for MPC spectroscopy. However, the additional noise due to the differentiation process is evident.

In addition to the peak in figure 5(b), a shoulder appears present on the deeper energy side. Two gaussian curves centred at 0.65 eV and 0.75 eV were found to fit the data taken at 390 K reasonably well. The area under the DOS peak measured at 390 K indicates a total density of states for these traps of 5×10^{15} cm^{-3}, with the shoulder amounting to 1×10^{15} cm^{-3}. It is unclear why such a large apparent variation in the DOS scale with temperature exists, a factor of around 10 between 350 K and 400 K. μ_n, C_n and α are known to be temperature-dependent, but a minor effect is expected over such a small temperature range.

There are several possible candidates for assignment of trap species at 0.65 eV and 0.75 eV below E_C in β-Ga_2O_3. Several studies [11, 15] have identified traps, denoted E2 (or E2* and E2) with energies in this range. E2* is associated with an intrinsic defect, either V_{Ga} or Ga_O, or possibly a divacancy (V_{Ga}-V_O). E2 is thought to correspond to a native point defect. Our intention here is to demonstrate the potential applicability of the MPC and CPM techniques to the study of traps in Ga_2O_3; readers seeking greater detail on assignments are referred to the literature cited herein.

3.2 CPM spectroscopy on α-Ga_2O_3

The CPM spectrum of α-Ga_2O_3 presented in Figure 6(a) is divided into 4 regions for the purpose of discussion, with the corresponding electronic transitions schematised in figure 6(b). The dark current activation energy lies in the range 0.6 to 1.0 eV, placing the dark Fermi level at a similar energy below the conduction band edge.

In region (i), photons above the bandgap energy (E_G > 5.1 eV) can excite electrons from all filled states to the CB. In a direct bandgap semiconductor, the DOS falls rapidly at the band edges,

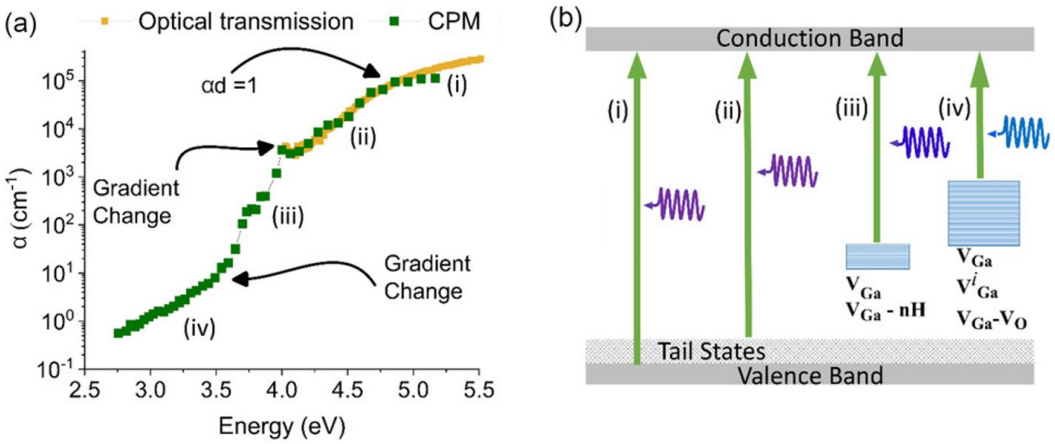

Figure 6. (a) CPM spectrum merged with optical transmission spectrum in vicinity of αd < 1. This serves to align and calibrate the CPM data. (b) Electron transitions from filled states (band states in VB, and localised states, including band tails and traps in the bandgap) to the CB give rise to photocurrent. Reprinted with permission from [27].

as does α, for $E_P < E_G$. If localised states extending from the valence band edge into the bandgap are present, α will fall less rapidly, broadening the absorption edge, which we see here in region (ii). This region has also been measured in β-Ga_2O_3 by Hao *et al* [28] using photothermal deflection spectroscopy and was found to have a characteristic slope energy of 120 meV. In our work we see a broader feature, of slope energy *ca*. 200 meV, which we attribute to the known presence of structural disorder and phase inclusions [29, 30] on defects in this range. It is also possible that broadening is associated with self-trapped holes, as proposed by Hao et al.

Region (iii), which covers energies from 3.6 eV to 4 eV, highlights the effectiveness of CPM as a probe of α in the sub-bandgap region. As discussed in section 1.4, the absolute accuracy of table-top optical transmission/reflection systems precludes accurate measurement of α if $\alpha d < 1\%$. In region (iii) α varies from 3000 cm^{-1} ($\alpha d = 7\%$) at 4 eV to 16 cm^{-1} ($\alpha d = 0.04\%$) at 3.6 eV, a much steeper slope than in region (ii). Several defects lying in this energy range have been proposed, with the low formation energy of the H-decorated V_{Ga} compared to isolated V_{Ga} [11] considered the most probable [31]. However, we see no evidence of sharp features in the CPM spectrum, such as the steps anticipated if discrete levels were present (see section 1.4). This suggests region (iii) may arise from V_{Ga}-nH complexes with exponentially-distributed trap energies.

In region (iv) the absorption coefficient decreases further, from 16 cm^{-1} at 3.6 eV to 0.8 cm^{-1} ($\alpha d = 0.0025\%$) at 2.7 eV, but with a shallower slope than in region (iii). It has been proposed that di-vacancies of V_{Ga} and V_O (V_{Ga}-V_O) would contribute states between 2.0 and 3.5 eV below E_C, depending on their charge state [32]. From a theoretical perspective, Varley *et al* have advanced the possibility of isolated V_{Ga} which relax to occupy interstitial sites, with energies calculated in the range of 2.1-3.3 eV below E_C, depending upon the charge state of the defect [31]. Therefore, we tentatively interpret region (iv) as arising from states involving V_{Ga}-V_O complexes, isolated V_{Ga} or relaxed V_{Ga} occupying interstitial sites, distributed over this energy range.

4. Conclusions

Interest in gallium oxide and related wide-bandgap alloys continues to grow, with commercial applications in power electronics and solar-blind photodetectors seemingly not far away. Understanding structure-property relationships, particularly the interplay between material deposition conditions, microstructure and defects, and their influence on electronic properties, is key to achieving systematic improvements in quality and development of new materials. Here we have outlined the main approaches to quantifying electronically-active defects (carrier traps) and explored the potential of two techniques new to the field of wide-bandgap semiconductor defect spectroscopy; Modulated Photo-Current Spectroscopy (MPC), and the Constant Photocurrent Method (CPM). While neither seems likely to displace the established techniques such as DLTS and DLOS, we have demonstrated their sensitivity to localised states in the bandgap of Ga_2O_3. Provided optical excitation is kept low, MPC is applicable to empty states (above the equilibrium Fermi level) and CPM to filled states. CPM permits quantitative measurement of the optical absorption coefficient across a broad wavelength range, over which routine optical methods are normally unsuitable. Detailed interpretation of results remains tentative, but is open to improvement by closer comparison with DLTS and other established defect spectroscopies. In contrast to DLTS/DLOS, which require fabrication of a Schottky or a p-n junction device, MPC and CPM are most suited to undoped bulk or film samples, suggesting a possible niche application, but on the other hand, defect charging and discharging cannot be controlled as for DLTS, and they are subject to state occupancy restrictions imposed by Fermi level position.

Acknowledgements

The authors acknowledge support from the Royal Society (RGS/R1/201236), the Engineering and Physical Sciences Research Council (EP/T517938/1, EP/V034995/1), and the UK Space Agency Enabling Technologies Programme (UKSAG23_0043_ETP4-052).

References

[1] Zhou H, Zhang J, Zhang C, Feng Q, Zhao S, Ma P and Hao Y A 2019 *J. Semicond.* **40** 011803
[2] Zhou J, Zhou X, Liu Q, Wong M H, Xu G, Yang S and Long S 2024 *IEEE Trans. Electron Devices* **71** 1513
[3] Yadava N and Chauhan R K 2020 *ECS J. Solid State Sci. Technol.* **9** 065010
[4] Chen X, Ren F, Gu S and Ye J 2019 P*hoton. Res.* **7** 381
[5] Xu J, Zheng W and Huang F 2019 *J. Mater. Chem. C* **7** 8753
[6] Akatsuka M, Kawaguchi Y, Itoh R, Ozawa A, Yamamoto M, Tanabe T and Yoshida T 2020 *Applied Catalysis B: Environmental* **262** 118247
[7] Zhu J, Xu Z, Ha S, Li D, Zhang K, Zhang H and Feng J 2022 *Materials* **15** 7339
[8] Higashiwaki M 2022 *AAPPS Bull.* **32** (3)
[9] Pearton S, Ren F and Mastro M (eds) Gallium Oxide Technology, Devices and Applications (Elsevier : Amsterdam) 2019
[10] McCluskey M D and Janotti, A 2020 *J. Appl. Phys.* **127** 190401
[11] Polyakov A Y, Nikolaev V I, Yakimov E B, Ren F, Pearton S J, Kim J 2022 *J. Vac. Sci. Technol. A* **40** 020804
[12] Fregolent M, De Santi C, Buffolo M, Higashiwaki, M, Meneghesso G, Zanoni E and Meneghini M 2021 *J. Appl. Phys.* **130** 245704
[13] Neal A T, Mou S, Lopez R, Li J V, Thomson D B, Chabak K D and Jessen H J 2017 *Scientific Reports* **7** 13218
[14] Polyakov A Y *et al* 2023 *ECS J. Solid State Sci. Technol.* **12** 045002
[15] Fregolent M *et al* 2024 *J. Phys. D: Appl. Phys.* **57** 433002
[16] Peaker A R, Markevich V P and Coutinho J 2018 *J. Appl. Phys.* **123** 161559
[17] Reynolds, S., Brinza, M., Benkhedir, M. L., & Adriaenssens, G. J. (2017). Photoconductivity in Materials Research. In Kasap, S. & Capper. P. (Eds.), Springer Handbook of Electronic and Photonic Materials (pp. 151-174) [Ch. 7]. Springer Handbooks. Springer, Cham.
[18] Rütten M, Geilen A, Sebastian A, Krebs D and Salinga M 2019 *Scientific Reports* **9** 6592
[19] Nakatsuka E, Kumoda Y, Mori K, Kobayashi T, Nagase T and Naito H 2020 *Materials* **13** 2660
[20] Vaněček, M, Kočka, J, Stuchlík, J and Tříska, A 1981 *Solid State Communications* **39** 1199
[21] Nandi A, Cherns D, Sanyal I and Kuball M 2023 *Cryst. Growth Des.* **23** 8290
[22] Reynolds S, Main C, Webb D P and Rose M J 2000 *Phil. Mag.* **B80** 547
[23] Brüggemann R, Main C, Berkin J and Reynolds S 1990 *Phil. Mag.* **B62** 29
[24] Hattori K, Niwano Y, Okamoto H and Hamakawa Y 1991 *J Non-Cryst. Solids* **137-138** 363
[25] Massabuau F P *et al* Progress in atomic layer deposited [alpha]-Ga2O3 materials and solar-blind detectors. In: *Oxide-based Materials and Devices XII 2021 Mar 5* (Vol. 11687, pp. 23-30). SPIE.
[26] Massabuau F, Nicol D, Adams F, Jarman J, Roberts J, Kovács A, Chalker P and Oliver R 2021 *J. Phys. D: Appl. Phys.* **54** 384001
[27] Nicol D, Reynolds S, Barr K, Roberts J W, Jarman, J, Chalker P and Massabuau F C-P 2024 *Physica Status Solidi (B) Basic Research* **261** 2300470
[28] Hao S, Hetzl M, Kunzelmann, V F, Matich S, Sai Q, Xia C, Sharp I D and Stutzmann M 2020 *Appl. Phys. Lett.* **116** 092102
[29] Roberts J W, Chalker P R, Ding B, Oliver R A, Gibbon J T, Jones L A H, Dhanak V R, Phillips L J, Major J D, Massabuau F C-P 2019 *Journal of Crystal Growth* **528** 125254
[30] Moloney J, Tesh O, Singh M, Roberts J W, Jarman J C, Lee L C, Huq T N, Brister J, Karboyan S, Kuball M, Chalker P R, Oliver R A, Massabuau F C-P 2019 *J. Phys. D: Appl. Phys.* **52** 475101
[31] Varley J B First-Principles Calculations 2: Doping and Defects in Ga2O3. In Gallium Oxide; Higashiwaki, M., Fujita, S., Eds.; Springer Series in Materials Science; Springer International Publishing: Cham, 2020; Vol. 293, pp 329–348
[32] Wang Z, Chen X, Ren F-F, Gu S, Ye J 2021 *J. Phys. D: Appl. Phys.* **54** 043002